Four-wave mixing in semiconductor optical amplifiers: physics and applications

Jianhui Zhou, Namkyoo Park, Kerry J. Vahala, Michael A. Newkirk, Barry I. Miller

Jianhui Zhou, Namkyoo Park, Kerry J. Vahala, Michael A. Newkirk, Barry I. Miller, "Four-wave mixing in semiconductor optical amplifiers: physics and applications," Proc. SPIE 2399, Physics and Simulation of Optoelectronic Devices III, (19 June 1995); doi: 10.1117/12.212536

SPIE.

Event: Photonics West '95, 1995, San Jose, CA, United States

Invited Paper

Four-Wave Mixing in Semiconductor Optical Amplifiers: Physics and Applications

Jianhui Zhou, Namkyoo Park*, Kerry J. Vahala
Department of Applied Physics, Mail Stop 128-95
California Institute of Technology, Pasadena, California 91125

Michael A. Newkirk† and Barry I. Miller
AT&T Bell Laboratories, Holmdel, New Jersey 07733

ABSTRACT

Nondegenerate four-wave mixing in semiconductor optical amplifiers was studied both as a spectroscopic tool for probing semiconductor dynamics and as a wavelength conversion technique. Four-wave mixing spectra were measured at detuning frequencies ranging from GHz to THz rates and ultrafast intraband mechanisms having relaxation time constants of 650 fs and less than 100 fs were revealed in the measurements. Cross-polarization four-wave mixing was also measured to study the inter quantum-well carrier transport process in quantum-well amplifiers. In addition, broadband wavelength conversion using four-wave mixing in semiconductor optical amplifiers was investigated. Results concerning the conversion efficiency over spans up to 65 nm, as well as a demonstration of wavelength conversion with gain are presented. The issue of converted signal-to-background noise in this process is also addressed.

Keywords: nonlinear wave mixing, semiconductor optical amplifier, intraband dynamics, inter quantum-well carrier transport, wavelength conversion, optical communications

1 Introduction

Nondegenerate four-wave mixing (FWM) in semiconductor optical amplifiers (SOA's) has been a topic of increasing interest over the past few years, both because of its use in understanding ultrafast semiconductor dynamics and its device applications in lightwave systems.[1-10] Two different physical processes have been found to cause FWM in semiconductor gain media. One is carrier density modulation induced by interband photomixing of the pump and probe fields. The other is ultrafast intraband dynamics, including dynamic carrier heating and spectral hole burning. Dynamic carrier heating results from stimulated emission, which removes "cold" carriers close to the band edges, and from free-carrier absorption, which transfers carriers to high energies within the bands. The hot carrier distributions relax to the lattice temperature by emission of optical phonons with a characteristic time constant of about $\sim$ 1 ps. Spectral hole burning refers to a spectrally local gain reduction due to the finite intraband carrier-carrier scattering time (<100 fs), which sets the time scale on which non-Fermi carrier distributions are restored to equilibrium.

*Present Address: AT&T Bell Laboratories, Murray Hill, New Jersey 07974
†Present Address: Ortel Corporation, Alhambra, California 91803

0-8194-1746-7/95/$6.00

Since the FWM signal spectra are essentially the frequency-domain response functions of the above mentioned contributing semiconductor dynamics, quantitative characterization of the FWM spectra can provide important information concerning these dynamics. Previously, its time-domain counterpart, pump-probe measurement using ultra-short optical pulses,[11-13] has been the only direct technique to probe ultrafast dynamics in semiconductor active layers. FWM spectroscopy of semiconductor dynamics presents data in a form that is complementary to these femtosecond studies, *i.e.* frequency domain rather than time-domain.

FWM in SOA's can also be used to achieve all-optical wavelength conversion which is an important functionality for future lightwave networks.[14-16] As the converted FWM signal is the phase-conjugate replica of the input signal, the conversion process is inherently transparent to the modulation format and bite rate and also provides the possibility of fiber-dispersion-compensation in lightwave communication systems.

In the next section, SOA FWM theory will be presented. In Section 3 FWM spectroscopy of ultrafast dynamics in semiconductor active layers is described, while in Section 4 inter quantum-well (QW) transport dynamics is studied using a novel cross-polarization FWM technique. Finally, broadband wavelength conversion using SOA FWM, including conversion efficiency and noise properties, is presented in Section 5. The conclusion is given in Section 6.

2 Theory

Let us assume that the pump, probe and the FWM signal all have the same polarization, and that these waves are given by,

$$\mathcal{E}_j(z,t) = E_j(z)\exp\left[i(k_j z - \omega_j t)\right] \tag{1}$$

where $j = p, q, s$ denote pump, probe and converted signals, respectively; $\{E_j(z)\}$ are the slowly-varying amplitudes of the three waves; and z is the longitudinal coordinate along the propagation direction. We can describe the propagation of these waves by means of coupled-amplitude equations. Assuming the validility of the slowly-varying-amplitude approach, and following procedures similar to those used in Agrawal's treatment,[17] we find that the slowly varying amplitudes must obey the following set of coupled equations,

$$\frac{dE_{p,q}(z)}{dz} = \frac{1}{2}\left(\frac{g_0}{1+\frac{P(z)}{P_s}}(1-i\alpha)-\alpha_l\right)E_{p,q}(z) \tag{2}$$

$$\frac{dE_s(z)}{dz} = \frac{1}{2}\left(\frac{g_0}{1+\frac{P(z)}{P_s}}(1-i\alpha)-\alpha_l\right)E_s(z) - \kappa(z)E_p^2(z)E_q^*(z)\exp(i\Delta k z) \tag{3}$$

where we have introduced the wave-number mismatch $\Delta k = 2k_p - k_q - k_s$ and a FWM coupling coefficient $\kappa(z)$. In addition, g_0 is the unsaturated optical gain per unit length, with its wavelength dependence neglected, $P(z)$ is the total optical power at position z in the waveguide, P_s is the SOA's saturation power, α is the linewidth enhancement factor and α_l is the SOA's nonsaturable internal loss per unit length. In deriving Eq. (2), we have neglected the power depletion of pump and probe waves, since, for detuning frequency larger than a few tens of GHz, the power transfer is negligible in comparison to the power in the pump and probe, themselves.

The coupling coefficient $\kappa(z)$ is of central importance to this theoretical analysis. To simplify the analysis, we treat the three possible mechanisms – carrier density modulation, dynamic carrier heating and spectral hole burning – as three independent processes. $\kappa(z)$ is found to be given by,

$$\kappa(z) = \frac{1}{2}\frac{g_0}{1+\frac{P(z)}{P_s}}\sum_{m=1}^{3}\frac{1-i\alpha_m}{1-i2\pi f\tau_m}\cdot\frac{1}{P_m} \tag{4}$$

where m=1, 2, 3, for carrier density modulation, dynamic carrier heating and spectral hole burning, respectively. f is the detuning frequency, defined as the difference between the optical frequencies of the pump (f_p) and probe

(f_q) waves; $\{\tau_m\}$ and $\{P_m\}$ are the lifetimes and saturation powers associated with the mechanisms; and $\{\alpha_m\}$ give the ratio between the real and the imaginary parts of the refractive index change induced by the mechanisms. Although a formal justification of the separation of the three mechanisms is possible based on the density matrix formalism,[18] it can be justified intuitively by noting that first, all interactions measured are in the small-signal regime in our FWM studies, and secondly, each relaxation mechanism results from bath damping from distinct, independent baths.

Using the boundary condition $E_s(0) = 0$, we solve Eqs. (2) and (3) and find that under moderate SOA saturation the converted signal amplitude at the SOA output ($z = l$) can be expressed by,

$$E_s(l) = -\frac{E_p^2(l)E_q^*(l)\kappa(l)le^{i\Delta kl}}{0.23G + i\Delta kl} \tag{5}$$

where $G = 4.34\int_0^l(\frac{g_0}{1+\frac{P(z)}{P_s}} - \alpha_l)dz$ is the SOA saturated gain in dB. The phase mismatch term can be expressed as $\Delta kl = \frac{\pi}{2}\cdot\frac{dn_g}{d\lambda}\cdot(\frac{\Delta\lambda}{\lambda})^2\cdot l$, where $\frac{dn_g}{d\lambda}$ is the group index dispersion. Using $\frac{dn_g}{d\lambda} \sim -0.7\mu m^{-1}$, measured by Hall *et. al.*,[19] and $l = 0.8$ mm for the devices in this study, the phase mismatch for $f = 1.7$ THz is estimated to be -0.27, which is negligible in comparison to the first term for a typical optical gain of $G \sim 15$ dB. Even for detuning frequencies up to 4 THz, the phase mismatch, -1.57, is still negligible.

Physically, the term $E_p(l)E_q^*(l)$ in Eq (5) represents the strength of the dynamic gratings induced by optical beating of pump and probe fields. An additional $E_p(l)$ arises from the fact that the FWM signal is generated through the scattering of the pump wave from these dynamic gratings. Since both pump and probe experience an optical gain of G, the SOA's single-pass gain acts three times in the expression for the FWM signal $E_s(l)$. This point is critical to implementation of efficient broadband wavelength conversion in SOA's.

3 Four-Wave Mixing Spectroscopy of Intraband Dynamics

FWM was measured on a strained InGaAs/InGaAsP MQW traveling-wave amplifier operating at 1.5 μm.[20] The SOA was measured to have a small-signal TM gain of about 20 dB and negligible gain ripple for a bias of 100 mA. Three single-frequency, tunable, Er-doped fiber lasers[21] were used in the measurement as pump, probe and local oscillators. These fiber lasers are unidirectional ring oscillators in which isolated, tandem fiber Fabry-Perot filters provide both tuning and mode selection.

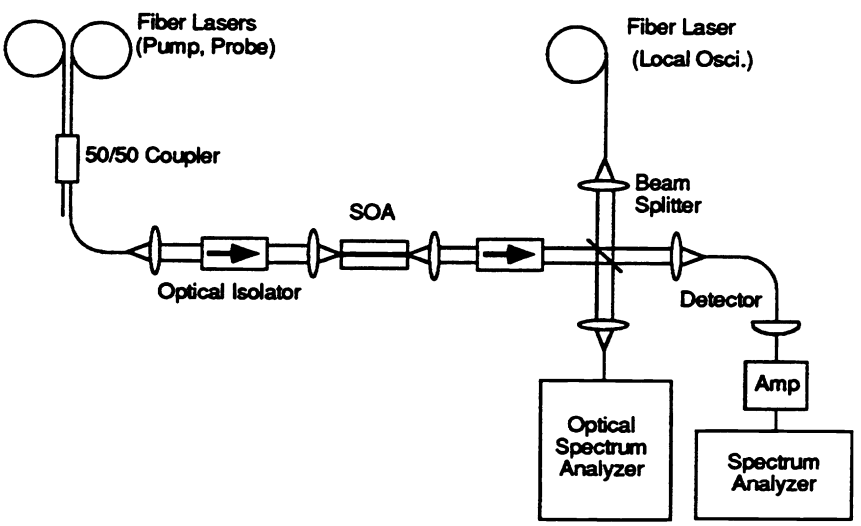

Fig.1 Experimental setup for the FWM measurement.

As shown in Fig. 1. the optical outputs from the pump and probe lasers were combined using a 3 dB fiber coupler, and then coupled into the SOA using microscope objectives. Two optical isolators, providing 60 dB isolation, were placed before and after the SOA to eliminate feedback caused by the facets of the input and output fibers, and also to select the TM polarization for the SOA input. During the measurements, the wavelength of the pump laser was fixed at 1534 nm, while the probe was tuned to vary the detuning frequency f. The FWM signal was heterodyne detected at a *pin* detector by mixing the signal with the fiber-laser local oscillator and tuning the local oscillator relative to the signal frequency. The IF mixing frequency was maintained at 4.00 GHz throughout the measurements, thereby ensuring the frequency response of detection electronics would not affect the measured results. The detected photocurrent was amplified by a microwave amplifier with 40 dB gain and then measured using a spectrum analyzer. The detuning frequencies were determined using an optical spectrum analyzer. The optical powers of pump, probe and local oscillator were also measured, so that the measured FWM signal could be normalized.

Using this experimental configuration, the FWM signal was measured for detuning frequency as high as 1.7 THz, limited only by the tunability of one of the fiber lasers used in the experiment. The normalized signal power as a function of detuning frequency is illustrated in Fig.2. Also shown in the figure are the theoretical fits that are obtained using the following expression for the normalized FWM signal power, as yielded by Eqs.(4) and (5),

$$I_s = |\sum_{j=1}^{3} C_j \cdot \frac{1}{1 - i2\pi f \tau_j}|^2 \tag{6}$$

The dashed line in Fig.2 represents the FWM response accounting only for carrier density modulation, *i.e.*, only the first term in Eq (6) is used. The deviation of the measured response from this one term fit indicates the presence of contributions from the intraband relaxation mechanisms. The asymmetric nature of the signal spectrum with respect to positive and negative detuning is believed to result from phase interferences which occur between the various contributing mechanisms. Since the positive detuning data show constructive interferences, we estimated a relaxation time constant of about 650 fs for an ultrafast intraband mechanism using the positive signal spectrum. We then try to fit the measured data with these two terms. However, as shown in Fig.2, the two term response is insufficient to provide a good fit over the whole signal spectrum. It was then found that a third term having a lifetime of less than 100 fs was required to obtain a good fit.

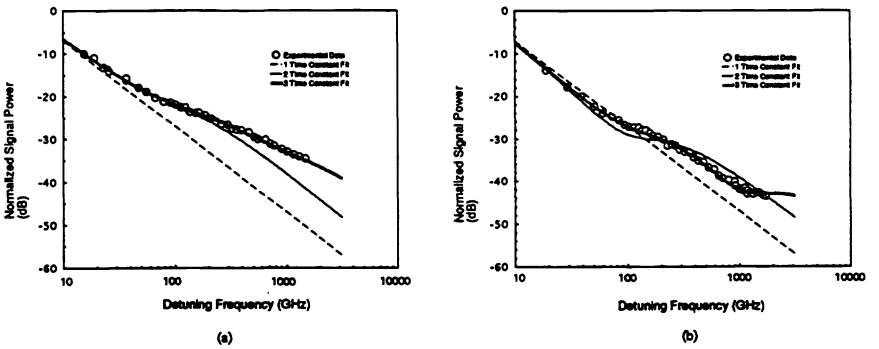

Fig.2 Normalized FWM signal power versus (a) positive, and (b) negative detuning frequencies showing theoretical fits.

Using Eq. (6), good fits were obtained for both positive and negative detuning data with the same parameter set (as shown in Fig.2 for the 3 term fit). The corresponding time constants used in Fig.2 are 200 ps, 650 fs and 50 fs. The time constant of 650 fs obtained in this study is in good agreement with the results of previous measurements of carrier heating in both time and frequency domains that have appeared in the literature.[1,11] The time constant for the ultrafast intraband mechanism used in the fit is 50 fs. However, it is important to note that the fit is insensitive to this parameter (empirically we can obtain good fits provided $\tau < 100$ fs) because the time resolution (or equivalently, the detuning frequency) is still limited in the measurements. Therefore, this time constant can not be given definite physical meaning in this study. However, the fact that a third term, having a time constant of less than 100 fs, is required to obtain a good fit clearly indicates the presence of additional ultrafast intraband processes. These are presumably related to spectral hole burning and the initial thermalization of carrier heating. They are based on the same carrier-carrier relaxation dynamics.[5,18]

Since gain and index gratings both contribute to the FWM process, the interpretation of FWM experimental results is somewhat more complicated than in the case of time-domain measurement, where gain and index contributions can be separated. However, the different interference behaviors present in positive and negative detuning signal spectra considerably facilitate theoretical analysis of the experimental data in FWM. Furthermore, the measurement presents data in a form that is complementary to femtosecond studies and is inherently a small signal approach. This latter point may explain the good agreement we find between a simple model and data.

4 Inter-Well Carrier Transport Probed by Four-Wave Mixing

Carrier transport in semiconductor QW lasers generally refers to capture and escape of carriers between unconfined three-dimensional (3-D) and confined two-dimensional (2-D) quantum states in the QW regions, and trans-barrier transport (*i.e.*, diffusion and drift of 3-D carriers) between wells in the barrier regions. Inter-well carrier transport in QW lasers has been shown to affect both the static and dynamic performance characteristics of these devices.[22-25] We present in this section the investigation of inter-well transport in an MQW SOA using a novel cross-polarization FWM technique. The SOA used in these measurements was a 1.5 μm MQW traveling-wave amplifier[26] whose active layer contains six alternating-strain (tensile and compressive) InGaAs QW's. As the tensile QW's provide predominantly TM gain, while the compressive QW's provide TE gain but have vanishing TM gain, this device enables selective excitation and probing of wells according to strain.

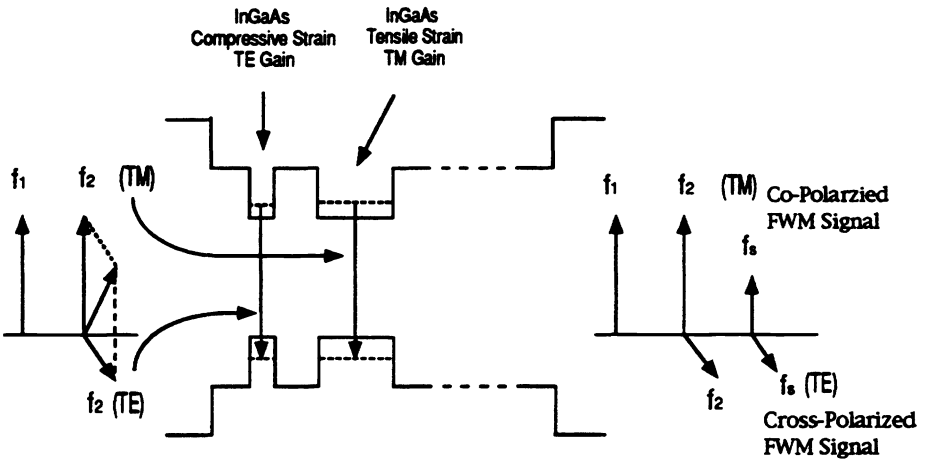

Fig.3 Diagram of FWM in SOA having a structure of alternating tensile and compressive QW's.

In a typical measurement, beam 1 having a given polarization (either TE or TM), and beam 2 having a polarization at an angle of 45 degrees with respect to beam 1, were coupled into the SOA. For the configuration shown in Fig.3, the beating between TM-polarized beam 1 and the TM component of beam 2 excites carriers in the tensile wells primarily through interband transitions. Carrier dynamics in the neighboring compressive QW's, which result from inter-well carrier transport, were then probed using the TE-polarized component of beam 2 (cross-polarization FWM), while carrier dynamics in the tensile QW's were probed using the TM-polarized component of beam 2 (co-polarization FWM). Fig.4 (a) and (b) show the measured cross-polarized (TM pump, TE probe) and co-polarized (TM pump and probe) FWM signal powers, normalized by the pump and probe amplitudes, plotted versus the detuning frequency. We also carried out co- and cross-polarization FWM measurements where pump waves were TE-polarized. The FWM signal spectra measured for this case are shown in Fig.4 (c) and (d).

Within an excited well, modulation is produced by the same mechanisms described in previous sections, but at the detuning frequencies of this measurement, inter-well transport includes primarily carrier number transport and carrier temperature transport. The inter-well carrier number transport can be approximately described as a three-step process. First, 2-D carriers in the excited well are coupled to the 3-D states of the same well

through quantum capture/escape processes. These 3-D carriers are then transported to the nonexcited wells through the combined effect of diffusion and drift. Finally, also through carrier capture/escape processes, the transported 3-D carriers fall into the 2-D states in the nonexcited well, where they contribute to the cross-polarized FWM. During the inter-well transport process, the two modulations (carrier number and temperature) experience different damping mechanisms, *i.e.*, transport of carrier number modulation is damped by spontaneous interband carrier recombination, while the carrier temperature modulation is damped by carrier-lattice interactions having a much shorter relaxation time. These widely different damping rates affect the corresponding inter-well transport efficiencies because of their strong dependence on damping.

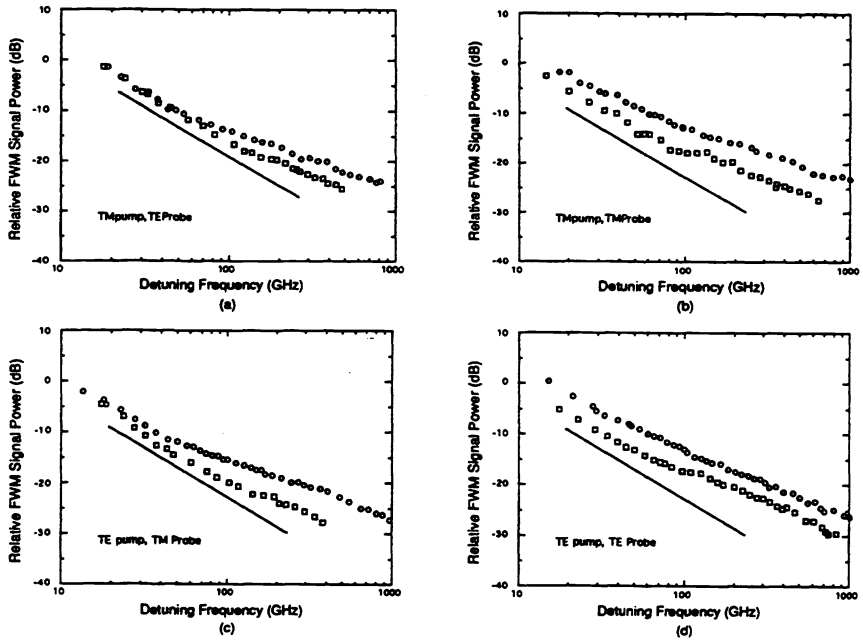

Fig.4 Normalized FWM signal power versus positive (○) and negative (□) detuning frequencies for various pump-probe polarization configurations:
(a) TM pump, TE probe
(b) TM pump, TM probe
(c) TE pump, TM probe
(d) TE pump, TE probe.

To illustrate, we calculate the trans-barrier transport efficiency by considering 3-D carrier transport from an excited well to the adjacent nonexcited well using a simple 1-D diffusion model. The trans-barrier transport efficiency is then given by,

$$\zeta = \exp\left(-\frac{s}{\sqrt{D}}\sqrt{\frac{1}{\tau_d} - i2\pi f}\right) \tag{7}$$

where D and τ_d are the diffusion constant and lifetime associated with either carrier number or temperature and s is the separation between wells. Since the carrier number damping time ($\sim$ 200 ps) is much longer than the temperature damping time ($\sim$ 650 fs), carrier temperature modulation transport is much less efficient than carrier number transport. Another contributing mechanism to the trans-barrier transport is drift of 3-D carriers caused by internal fields. The drift process, like the diffusion process, also favors the mechanism having the longer time constant so that, assuming all other factors are comparable, carrier number transport is again expected to be more efficient than the carrier temperature transport.

Similarly, the efficiency associated with the escape/capture dynamics are also subject to the damping effect. Widely different relaxation time constants for the two modulations should lead to very different efficiencies in the escape/capture process. We would therefore expect overall inter-well transport to exhibit a higher efficiency for the carrier number modulation than for the temperature modulation. As shown in Fig.4, the cross- and co-polarized FWM signals were found to have comparable amplitudes at low frequencies. Furthermore, the cross-polarized FWM data in Fig.4 (a) and (c) do not show any roll-off induced by the carrier number transport (*i.e.*, beyond the 20 dB/decade roll-off caused by the interband modulation within the excited wells). This indicates that carrier number modulation, which is responsible for the low frequency data, is coupled efficiently from excited wells to nonexcited wells. This agrees qualitatively with a calculation of the trans-barrier transport efficiency

function which gives $|\zeta| > 78\%$ for $\tau = 200$ ps, $D = 5$ cm^{2}s^{-1}, $s = 100$ Å and $f < 100$ GHz. It also suggests that the inter-well carrier-number transport in the present device is fast enough so that carrier number modulation in nonexcited wells behaves as if it were generated within these wells for frequencies at least as high as 100 GHz. Beyond this frequency the modulation data is obscured by the presence of additional mechanisms, making prediction of a definitive upper transport rate impossible.

The cross-polarized FWM signal spectra are symmetrical at low frequencies with respect to positive and negative detuning in contrast to the co-polarized FWM spectra, which show a steady asymmetry. As shown in the above calculation and discussion, transport of carrier number modulation should be much more efficient than the transport of temperature modulation, especially at frequencies lower than the corner frequency of the carrier heating effect ($\sim$ 250 GHz). (As indicated in Eq. (7), the trans-barrier transport efficiencies become comparable beyond this frequency.) Phase interferences are therefore suppressed in the cross-polarized measurement at low frequencies, causing the highly symmetrical spectra.

Finally, it should be mentioned that carrier heating induced by free-carrier absorption is not strain selective. Specifically, it can take place in both types of wells when pumps are TE polarized, but it is inhibited in all wells when pumps are TM polarized due to the QW confinement barrier. Therefore, temperature modulation within the nonexcited wells is potentially significant in the case of TE pumps. This might explain the observed difference in the two sets of cross-polarized spectra at low detuning frequencies, where data with TE pumps show an earlier onset of reduced symmetry (*i.e.*, more phase interference between carrier number and temperature modulations).

5 Wavelength Conversion

Wavelength conversion is recognized as an important function in future broadband multichannel lightwave systems, since it makes possible many other useful system functions such as wavelength reuse and dynamic wavelength routing and switching.[14-16] Using FWM in SOA's to translate optical carriers from one wavelength to another (*i.e.*, wavelength conversion) has a number of advantages, including, for example, transparency to modulation format and bite rate. In this section we present our results showing conversion over wavelength spans up to 65 nm, as well as a demonstration of lossless wavelength conversion using a tandem SOA structure. In addition, we discuss and measure the signal to background noise ratio and present a noise reduction technique using a selective noise filter.

5.1 Conversion Efficiency

Using Eq. (5), SOA FWM wavelength conversion efficiency can be expressed by the simple relation:

$$\eta = 3G + 2I_p + R(\Delta\lambda) \tag{8}$$

where η is the ratio in dB of the converted signal output power to the signal input power and G is the saturated SOA optical gain.Other parameters appearing in Eq. (8) include the input optical pump-wave power I_p (expressed in dBm), and a quantity we call the relative efficiency function, $R(\Delta\lambda)$, which is given by,

$$R(\Delta\lambda) = 20\log\left|\sum_{m=1}^{3} c_m \cdot \frac{1}{1 - i2\pi f\tau_m}\right| \tag{9}$$

where, as discussed earlier, the three terms in the summation represent contributions to FWM wavelength conversion from the responsible mechanisms. $\Delta\lambda$ is the wavelength shift related to detuning frequency by $\Delta\lambda = -2\lambda^2 f/c$.

A crucial point is the presence of $3G$ in this expression. This occurs because the nonlinear field mixing involved in the FWM process uses the pump wave twice and the input signal once so that overall the amplifier's

single-pass gain acts three times. As an aside, we note that $3G$ in Eq. (8) assumes equal gain for pump and signal waves. In general, we have $2G_p + G_q$ where G_p and G_q are pump and input signal gains, respectively. In the present measurement, we employed a novel tandem amplifier geometry in which two or three SOA's, separated by optical isolators, were placed in series. Although not intended as a practical converter, the tandem geometry provides a simple method for realizing higher optical gains and testing theoretical predictions concerning conversion efficiency.

We first measured the dependence of the conversion efficiency η on the saturated single-pass SOA gain G. For this measurement, wavelengths and powers of the pump and signal waves remained fixed, and the single-pass gain was varied by changing the bias currents of the two SOA's between 80 mA and 175 mA. Shown in Fig.5 is typical conversion efficiency data plotted versus single-pass saturated optical gain. Conversion was measured from 1532.0 nm to 1523.0 nm with a pump power of −5.2 dBm and an input signal power of −11.3 dBm. Over this wavelength span, G has negligible wavelength dependence. The measured slope of 3.18 verified the cubic dependence of efficiency on single-pass gain. Similar values for the slope were obtained for many other wavelength shifts and input power levels.

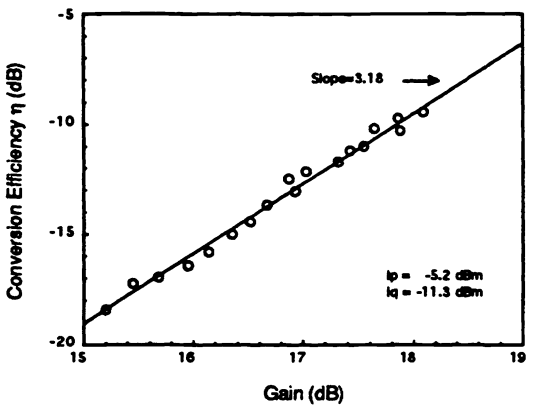

Fig.5 Measured conversion efficiency η versus SOA gain, showing the cubic dependence.

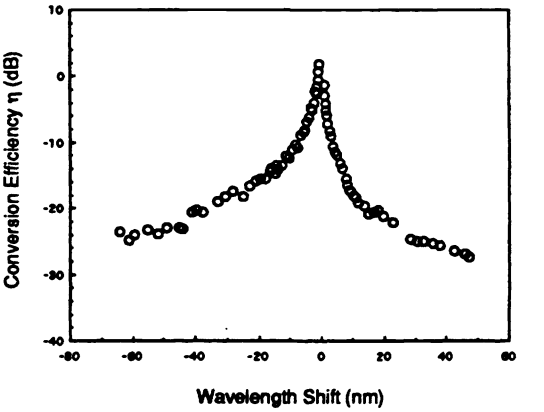

Fig. 6 Measured conversion efficiency η versus wavelength shift $\Delta\lambda$ (tandem amplifier with 2 SOA's).

The wavelength-shift dependence of the conversion process was also measured for both wavelength up- and down-conversion. In the down-conversion experiment, the pump was fixed at 1526.0 nm with −5.3 dBm of power coupled into the SOA wavelength converter. The maximum wavelength down-shift measured in this study was as large as 65 nm, corresponding to a frequency shift of 8 THz. In the up-conversion measurement, the pump was fixed at 1549.0 nm with a power of −6.0 dBm. Wavelength up-conversion was measured for shifts up to 47.5 nm, corresponding to a frequency shift of -6 THz. The conversion efficiency η for both positive and negative wavelength shifts is presented in Fig.6, where the efficiency is normalized using the typical parameter values in this study: pump power of −5.5 dBm, signal power of −10 dBm and saturated optical gain G of 18.2 dB (corresponding to the total input power). The normalization may introduce a small, but negligible error arising from slight spectral variation in the saturated SOA gain for the pump and input signal over the wavelength spans measured. An efficiency asymmetry with respect to positive and negative wavelength shifts is caused by phase interferences which occur between the various contributing inter- and intraband FWM mechanisms. The measurement of wavelength conversion up to 65 nm shows that ultrafast FWM dynamics in SOA's are capable of generating converted signals over very large wavelength spans.

In a separate tandem amplifier measurement where three SOA's were used, we achieved η >0 dB, *i.e.*, wavelength conversion with gain. The measured conversion efficiencies versus wavelength shift are presented in Fig.7 for a pump power of −11.5 dBm and a signal power of −15.2 dBm (SOA optical gain G was saturated to 24.2 dB at this input pump level). Conversion efficiencies greater than 0 dB (conversion with amplification), as shown in Fig.7, were achieved for down-conversion up to $\sim$ 7.0 nm and for up-conversion over $\sim$ 2.0 nm. In addition, conversion efficiency remained as high as 14% for down-conversion shifts as large as 23.9 nm. This is the first

demonstration of broadband SOA FWM wavelength conversion with amplification, indicating high conversion efficiency is possible with SOA FWM wavelength converters.

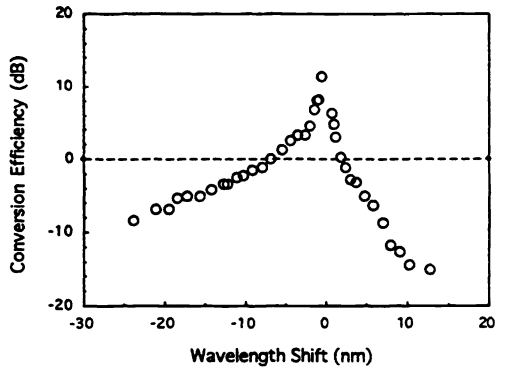

Fig. 7 Measured conversion efficiency η versus wavelength shift $\Delta\lambda$ (tandem amplifier with 3 SOA's).

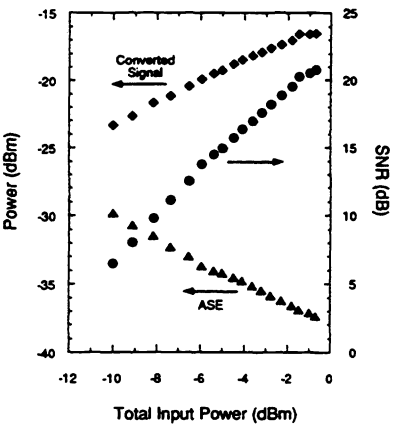

Fig. 8 Measured FWM signal power, spontaneous noise, SNR versus total input power.

5.2 Signal to Noise Performance

The ratio of converted signal to amplified spontaneous emission (ASE) noise (SNR) is another important parameter for a wavelength converter. In the first experiment that we described in the above section, SNR (ASE noise normalized to a 0.1 nm bandwidth) for a total input power level of -4.2 dBm (as used in Fig.6) was measured to be about 15 dB for -5 nm of shift and steadily dropped to 0 dB slightly beyond -65 nm of shift. However, improvement in the SNR can be expected with higher total input power (pump + input signal) because SNR increases with the total input power. Shown in Fig.8 is measured converted signal power, ASE noise power (normalized 0.1 nm bandwidth), and SNR as a function of total input power for a 5 nm wavelength down shift. The maximum SNR is 20.8 dB for -0.7 dBm of total input power. It results because of reduction of amplified spontaneous emission noise in conjunction with increasing converted signal power as the amplifier saturates. The fact that converted signal power continues to increase in this regime is due to its cubic dependence on total output power at a fixed pump to signal power ratio, as indicated in Eq. (5).

In SOA FWM wavelength conversion demonstrations to date, either the input signal is preamplified by an erbium-doped fiber amplifier (EDFA) before being coupled into the SOA mixer,[6,8] or, as described in the previous section, a tandem SOA structure which provides high single-pass gain is used. In the latter case, the first SOA serves as a preamplifier since the nonlinear mixing takes place primarily in the last segment of the tandem amplifier where the pump and input signal fields are strongest. The preamplification which occurs in each of these approaches is crucial to improving overall converter performance, since converter efficiency depends on the cube of any preamplification gain.[9,10] Spontaneous noise from the preamplification stage that resides in the conversion frequency band, however, constitutes a major part of the noise at the converter's output. We refer to this component as the "direct" noise component. Unlike normal applications of optical preamplifiers in which amplification and spontaneous noise are inextricably connected, direct spontaneous noise associated with optical preamplification can, in principle, be eliminated, thereby vastly improving overall converter function. This can be done by introducing a filter between the preamplifier and the mixer which removes the preamplifier spontaneous noise component in the spectral vicinity of converted signal wavelength.

The spontaneous noise power spectral density of one polarization at the mixer's output can be written as,

$$S^m_{out}(\lambda) = G_m S^m_{in}(\lambda) + \eta_m(\Delta\lambda) S^m_{in}(\lambda - \Delta\lambda) + n^m_{sp}\left(G_m - 1\right) h\nu \qquad (10)$$

where G_m and n^m_{sp} are the SOA's saturated single pass gain and spontaneous emission factor, respectively; $\eta_m(\Delta\lambda)$ is the conversion efficiency of the SOA mixer for wavelength shift $\Delta\lambda$, defined as the ratio of converted signal

power at the mixer's output to input signal power coupled into the mixer. Physically, the three terms on the right side in Eq. (10) represent amplified input noise, converted input noise, and ASE noise introduced by the SOA mixer, respectively.

We note that among the three contributions to the output spontaneous noise shown in Eq. (10) the direct noise can be reduced by selective filtering between the preamplifier and the mixer. This is possible since removal of noise components at the converted signal band at the mixer's input will have no effect on the subsequent mixing process. Such a filter which attenuates the converted signal bands by a factor of γ but leaves the input signal and pump bands unaffected will cause a spontaneous noise reduction in dB given by,

$$\text{Noise Reduction} = 10\log\frac{S_{in}^m + \frac{1}{2}F_n^m h\nu}{S_{in}^m/\gamma + \frac{1}{2}F_n^m h\nu} \tag{11}$$

where $F_n^m = 2n_{sp}^m\left(1 - \frac{1}{G_m}\right)$ is the SOA mixer's amplification noise figure. The converted input noise, which is normally much smaller than the amplified noise and the ASE introduced by the mixer, has been ignored in Eq. (11). It should be noted, however, that this converted noise would be the only remaining noise in an optimal converter scheme, as will be discussed later in this paper.

Since the ASE noise introduced by the SOA mixer can be written as $\frac{1}{2}G_m F_n^m h\nu$, the term $\frac{1}{2}F_n^m h\nu$ can be viewed as the equivalent input noise power spectral density of the SOA mixer. Using $F_n^m = 8$ dB and $h\nu = 0.809$ eV the calculated noise reduction is plotted in Fig.9 versus S_{in}^m for various filter extinction ratios γ. The effectiveness of this noise reduction technique, as indicated in the equation and Fig.9, strongly depends on the relative magnitude of the input noise power spectral density S_{in}^m coupled into the SOA mixer and the equivalent input noise power spectral density of the SOA mixer $\frac{1}{2}F_n^m h\nu$. The former, in turn, strongly depends on preamplification gain, and the latter depends on the SOA mixer's noise as characterized by its amplification noise figure.

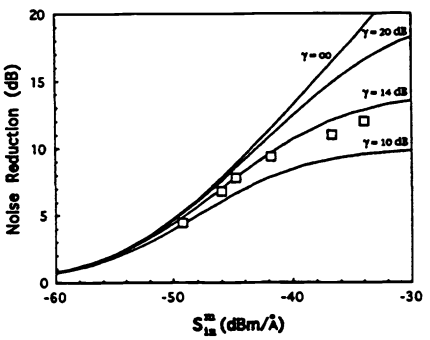

Fig. 9 Noise reduction versus the spontaneous noise power density s_{in}^m at the SOA mixer's input.

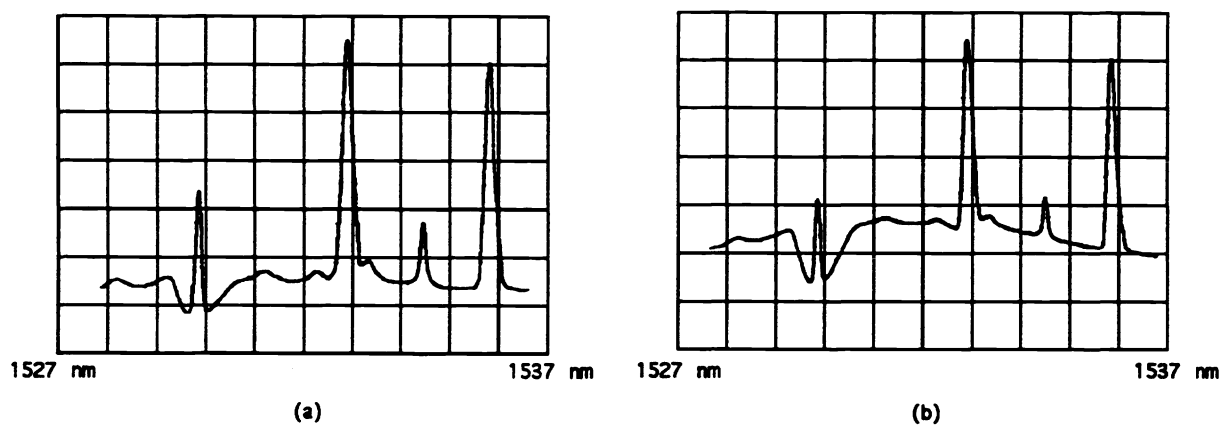

Fig. 10 Spectra of the SOA mixer's output for (a) $s_{in}^m = -46.0$ dBm and (b) $s_{in}^m = -36.7$ dBm showing spontaneous noise reduction. The small peak between the pump and input signal is a side mode of the DFB laser output. Vertical scale: 10 dB/div; Horizontal scale: 1 nm/div.

We have experimentally verified this idea. A tunable erbium-doped fiber ring laser and a DFB laser were used as pump and input signal sources. The SOA mixer was a tensile strained InGaAs MQW amplifier operating at 1.5 μm.[20] An EDFA was used as the preamplifier for both the input signal and pump, followed by a fiber notch filter having a 0.96 nm bandwidth, a 14 dB extinction ratio centered at 1.53 nm and near unity transmission outside of the filter band. The total optical power of input signal and pump into the preamplifier was attenuated to vary the EDFA gain and thus the spontaneous noise power spectral density S_{in}^m. The measured noise reduction versus S_{in}^m is presented in Fig.9 and is in good agreement with theory. Fig.10 shows measured spectra of the SOA mixer's output where significant noise reduction is visible.

The theoretical analysis and measurements described in this paper also suggest new considerations for optimal converter structures. Overall optical gain of the preamplifier and the SOA mixer has been previously shown to be crucial for high conversion efficiency performance. However, ASE noise introduced in the conversion process can considerably degrade the signal to noise ratio. To combat this problem, we propose to completely separate the functions of gain and nonlinearity. In an optimal converter structure, the first stage would consist of two preamplifiers, either EDFA's or SOA's, for the pump and input signal, respectively. Separate amplification of pump and input signal is advantageous because of better noise performance. Each of the preamplifiers is followed by a noise filter that removes spontaneous noise outside the pump band or input signal band. The third stage of the wavelength converter is the nonlinear mixer, which can be a highly saturated SOA, or a properly designed semiconductor waveguide with energy gap greater than the photon energy ($E_{gap} > h\nu$). In the former case the introduced ASE noise, as given by $n_{sp}^m(G_m - 1)h\nu$, depends on the SOA mixer saturation level, while in the latter case there will be virtually no ASE noise introduced by the mixer.

With this proposed structure, the high-gain preamplifiers provide high optical power into the mixer thereby maintaining efficient wavelength conversion in the mixer, however, they do not significantly contribute to the output spontaneous noise since filters can, in principle, eliminate the direct ASE noise in the converted signal band. Ideally, by using below gap mixing, only the converted ASE noise would remain in Eq (10). This would mean that signal to noise degradation would occur primarily in the preamplifiers, provided that the subsequent nonlinear wave mixing is efficient enough to maintain the noise level at the mixer output above the standard quantum limit. The mixing efficiency depends not only on the mixer's intrinsic parameters including the third order susceptibility and interaction length, but also on the preamplifier gain which determines powers of the pump and input signal at the mixer input. High gain preamplifiers are therefore also crucial to the noise performance of the overall conversion process.

6 Conclusion

We have described FWM spectroscopy of SOA's in the THz regime. A time constant of 650 fs in agreement with dynamic carrier heating was determined. The experimental data also indicate the presence of an ultrafast process with a lifetime less than 100 fs. Using a novel cross-polarization FWM configuration, inter-well carrier transport was investigated and the trans-barrier transport rate was estimated to be faster than 100 GHz. We have also presented our study of wavelength conversion based on SOA FWM. Conversion efficiency and noise properties were measured and discussed. We also described a noise reduction scheme in which a noise filter is placed before the SOA mixer. This idea was verified in a experiment and also lead to a suggestion of separation of gain and nonlinearity in an optimal converter structure.

7 Acknowledgments

The authors wish to thank W. W. Morey of United Technology Research Center for the fiber grating notch filter used in the noise reduction measurement. This work was supported by the Advanced Research Program

Agency (Contract #NDAAL01-94-K-03430), the National Science Foundation (Contract #ECS-9412862) and the Office of Naval Research (Contract #N00014-91-1524).

8 REFERENCES

[1] L. F. Tiemeijer, *Appl. Phys. Lett.*, **59**, 499 (1991).

[2] K. Kikuchi, M. Kakui, C. E. Zah, and T. P. Lee, *IEEE J. Quantum Electron.*, **28**, 151 (1992).

[3] J. Zhou, N. Park, J. W. Dawson, K. J. Vahala, M. A. Newkirk, and B. I. Miller, *Appl. Phys. Lett.*, **63**, 1179 (1993).

[4] A. D'Ottavi, E. Iannone, A. Mecozzi, S. Scotti, P. Spano, J. Landreau, a. Ougazzaden, and J. C. Bouley, *Appl. Phys. Lett.*, **64**, 2492 (1994).

[5] A. Uskov, J. Mφrk, J. Mark, M. C. Tatham and G. Sherlock, *Appl. Phys. Lett.*, **65**, 944 (1994).

[6] M. C. Tatham, G. Sherlock, and L. D. Westbrook, *IEEE Photon. Technol. Lett.*, **5**, 1303 (1993).

[7] J. Zhou, N. Park, J. W. Dawson, K. J. Vahala, M. A. Newkirk, and B. I. Miller, *IEEE Photon. Technol. Lett.*, **6**, 50 (1994).

[8] R. Ludwig, and G. Raybon, *Electron. Lett.*, **30**, 338 (1994).

[9] J. Zhou, N. Park, K. J. Vahala, M. A. Newkirk, and B. I. Miller, *IEEE Photon. Technol. Lett.*, **6**, 984 (1994).

[10] J. Zhou, N. Park, K. J. Vahala, M. A. Newkirk, and B. I. Miller, *Electron. Lett.*, **30**, 859 (1994).

[11] K. L. Hall, J. Mark, E. P. Ippen, and G. Eisenstein, *Appl. Phys. Lett.*, **56**, 1740 (1990).

[12] J. Mark and J. Mφrk, *Appl. Phys. Lett.*, **61**, 9 (1992).

[13] K. L. Hall, G. Lenz, E. P. Ippen, U. Koren, and G. Raybon, *Appl. Phys. Lett.*, **61**, 2512 (1992).

[14] S. B. Alexander, et. al., *IEEE J. Lightwave Technol.*, **11**, 714 (1993).

[15] C. A. Brackett, *et al.*, *IEEE J. Lightwave Technol.*, **11**, 736 (1993).

[16] K. -C. Lee, and V. O. K. Li, *IEEE J. Lightwave Technol.*, **11**, 962 (1993).

[17] G. P. Agrawal, *J. Opt. Soc. Am. B*, **5**, 147, (1988).

[18] A. Uskov, J. Mφrk, and J. Mark, *IEEE J. Quantum Electron.* **30**, 1769 (1994)

[19] K. L. Hall, G. Lenz, and E. P. Ippen, *IEEE J. Lightwave Technol.*, **10**, 616 (1992).

[20] B. I. Miller, U. Koren, M. A. Newkirk, M. G. Young, R. M. Jopson, R. M. Derosier and M. D. Chien, *IEEE Photon. Technol. Lett.*, **5**, 520 (1993).

[21] N. Park, J. W. Dawson, K. J. Vahala, and C. Miller, *Appl. Phys. Lett.*, **59**, 2369 (1991).

[22] W. Rideout, W. F. Sharfin, E. S. Koteles, M. O. Vassell, and B. Elman, *IEEE Photon. Tech. Lett.*, **3**, 784 (1991).

[23] R. Nagarajan, T. Fukushima, S. W. Corzine, and J. E. Bowers, *Appl. Phys. Lett.* **59**, 1835 (1991).

[24] S. C. Kan, D. Vassilovski, T. C. Wu, and K. Y. Lau, *Appl. Phys. Lett.* **63**, 2307 (1993).

[25] N. Tessler, and E. Eisenstein, *IEEE J. Quantum Electron.*, **29**, 2230 (1993).

[26] M. A. Newkirk, B. I. Miller, U. Koren, M. G. Young, M. Chen, R. M. Jopson, and C. A. Burrus, *IEEE Photon. Tech. Lett.*, **5**, 406 (1993).